Electronic Supplementary Material (ESI) for Nanoscale.

Supporting Information

Janus polymer-grafted nanoparticles mimicking membrane repair proteins for prevention of lipid membrane rupture

Bin Li,[a] Huimin Gao,*[a] and Zhong-Yuan Lu*[a]

[a] *State Key Laboratory of Supramolecular Structure and Materials, Institute of Theoretical Chemistry, Jilin University, Changchun 130023, China.*
E-mail: gaohuimin@jlu.edu.cn; luzhy@jlu.edu.cn

Model and Simulation Details

We use dissipative particle dynamics (DPD) simulation method in this study[1–3]. In DPD, the time evolution of coarse-grained beads is governed by Newton's equations of motion[4],

$$\frac{dr_i}{dt} = v_i, \tag{S1}$$

and

$$m\frac{dv_i}{dt} = f_i, \tag{S2}$$

where r_i, v_i and f_i are, respectively, the position, velocity and force on the i-th bead with mass m at time t. The force acting on bead i by bead j contains three non-bonded pairwise forces, i.e.,

$$f_i = \sum_{i \neq j} (F_{ij}^C + F_{ij}^D + F_{ij}^R), \tag{S3}$$

including the conservative force F_{ij}^C , dissipative force F_{ij}^D , and random force F_{ij}^R. They are given, respectively, as follows:

$$F_{ij}^C = \begin{cases} \alpha_{ij}\left(1 - \frac{r_{ij}}{r_c}\right)e_{ij} & r_{ij} < r_c, \\ 0 & r_{ij} \geq r_c, \end{cases} \tag{S4}$$

$$F_{ij}^D = -\gamma\omega^D(r_{ij})(v_{ij} \cdot e_{ij})e_{ij}, \tag{S5}$$

and

$$F_{ij}^R = \sigma\omega^R(r_{ij})\xi_{ij}\Delta t^{-\frac{1}{2}}e_{ij}, \tag{S6}$$

where $\mathbf{r}_{ij} = \mathbf{r}_i - \mathbf{r}_j$, $r_{ij} = |\mathbf{r}_{ij}|$, $\mathbf{e}_{ij} = \mathbf{r}_{ij}/r_{ij}$, $\mathbf{v}_{ij} = \mathbf{v}_i - \mathbf{v}_j$, α_{ij} represents the maximum repulsion between interacting beads i and j. ω^D and ω^R are weight functions for the dissipative and random forces, respectively. γ is a friction coefficient, which indicates the strength of the dissipative interaction between the particles of the system. σ represents the noise intensity. They are related via the fluctuation-dissipation theorem[1,5]

$$\sigma^2 = 2\gamma k_B T, \tag{S7}$$

$$\omega^D(r_{ij}) = [\omega^R(r_{ij})]^2 = \begin{cases} \left(1 - \frac{r_{ij}}{r_c}\right)^2 & r_{ij} < r_c, \\ 0 & r_{ij} \geq r_c. \end{cases} \tag{S8}$$

k_B is the Boltzmann constant and T is the absolute temperature of the system. In Eq. (S6), ξ_{ij} is a random number with zero mean and unit variance. These forces are of short-range with a fixed cutoff distance r_c. The Groot-Warren-velocity-Verlet algorithm[1,6] is used here to integrate Newton's equations of motion. For simplicity, we choose the bead mass m, the cutoff distance r_c, and the kinetic energy k_BT as units: $m = r_c = k_BT = 1$. Therefore, the relevant time unit is $\tau = (m\, r_c^2/k_BT)^{\frac{1}{2}} = 1$. In our simulations, we set the number density of the system $\rho = 3$, and the integration time step $\Delta t = 0.02$. Unless specified otherwise, all dimensional values are given in DPD reduced units.

When modeling lipids and polymer grafted chains, the bonds between beads in the chain are described via the harmonic spring potential

$$U_{bond}(r) = \frac{1}{2}k_b(r - r_0)^2. \tag{S9}$$

Here k_b is the spring constant and r_0 is the equilibrium bond length. According to Ref.[7], we set $k_b = 128$ and $r_0 = 0.5$. In the previous studies of Xia et al.[8,9], Alexeev et al.[7] and Ni et al.[10], they have demonstrated that applying a weaker bond between the first hydrophobic beads on the two tails of the lipids is a rational means to maintain the same directionality of the hydrophobic tails but not to change the function of the bilayer membrane. We thus take the same means to limit the directionality of the hydrophobic tails of the lipid, and we introduce a weaker bond ($k_b = 32$) between the first hydrophobic beads on the two tails of the lipid. We also introduce a three-body bond angle potential to describe the rigidity of lipid tails.

$$U_{angle} = k_a(1 + \cos\theta), \tag{S10}$$

where k_a is the bond angle force constant, θ is the the angle formed by three adjacent beads. We set $k_a = 20$ and $\theta = 180$ in this study.

The amphiphilicity of the lipids is captured by specifying repulsive interactions between different components. For any two beads of the same type (except for NP), we set the repulsion parameter to $\alpha_{ii} = 25$. Considering the rigid structure of the Janus NP and the non-interpenetration of the beads, we set $\alpha_{NN} = 100$[11]. Hence, α_{ij} will be larger than 25 when the bead-bead repulsion interaction is stronger. Suitable combination of these parameters can effectively illustrate the driving force for the self-assembly in water. Given that H stands for the hydrophilic lipid head, T stands for the hydrophobic lipid tail and W stands for the water (the solvent), we take the interaction parameter $\alpha_{HW} = 25$, $\alpha_{TW} = 100$ and $\alpha_{TH} = 100$. These values are found to give well-ordered membrane bilayer structure

of the lipids in water[7]. Other interaction parameters in the present simulations are carefully selected based on the properties and interactions of different beads. In this work, we attempted to construct a model of Janus PGNPs that can effectively mimic the behavior of repair proteins, that is, the PGNPs can specifically adsorb to the pore of damaged lipid membrane and then shed automatically after the membrane repair. In view of this, the parameters (α_{ij}) were carefully set to satisfy the following aspects: 1) normally, the hydrophilic chains of amphiphilic PGNPs should make the PGNPs stable in the solvent and meanwhile have a strong exclusion to the lipid hydrophobic layer, both of which contributes to ensuring the lowest impact of the introduced PGNPs on the lipid bilayer structure. Here, we refer to the work of Xu et al.[12] to set the parameters of the graft chain interactions; 2) as for the hydrophobic chains of PGNPs, their affinity to the hydrophobic tail of lipid membrane should be strong enough to drive the adsorption of PGNPs to the pore edge of damaged membrane; 3) when the lipid membrane is restored to its initial state, the repulsion between the hydrophobic chains of PGNPs and the lipid hydrophilic head, as well as the attraction of the solvent to the hydrophilic chains of PGNPs, should collectively promote the shedding of PGNPs. Based on the above considerations, in combined with our and others' previous research works[13], we made small adjustments by referring to the parameters of the solvent and the lipid membrane, and finally determined the parameters in the article, as listed in Table S1.

Generally, the value of the hydrophilic and hydrophobic parameters corresponds to a certain category of substances, which can be corrected according to the relationship between α_{ij} and the Flory–Huggins χ-parameters, that is, $\alpha_{ij} = \alpha_{ii} + 3.27\ \chi_{ij}$[14]. We have calibrated the Flory-Huggins parameters between different types of beads, as shown in Table S2.

Table S1 DPD interaction parameters used in the simulations

$\alpha_{ij}(k_BT/r_c)$	H	T	N	A	B	W
H	25.0	100.0	40.0	60.0	25.0	25.0
T		25.0	40.0	25.0	40.0	100.0
N			100.0	60.0	60.0	25.0
A				25.0	40.0	30.0
B					25.0	25.0
W						25.0

Table S2 Flory–Huggins χ-parameters used in the simulations

$\chi_{ij}(k_BT/r_c)$	H	T	N	A	B	W
H	0.0	22.9	4.6	10.7	0.0	0.0
T		0.0	4.6	0.0	4.6	22.9
N			22.9	10.7	10.7	0.0
A				0.0	4.6	1.5
B					0.0	0.0
W						0.0

In our system, each lipid molecule is modeled as an amphiphilic molecule consisting of three hydrophilic head beads (H, blue) and two tails with respective three hydrophobic beads (T, pink and cyan, Fig. 1(a) in the paper). The nanoparticle (NP, orange) is constructed via the geodesic subdivision method. In practice, to make sure the NP is impenetrable, we generate an outer shell and an inner shell with slight radius difference (e.g., $R_{outer} - R_{inner} = 0.5r_c$). In each shell, the surface density of the NP-type beads is 3.0. This two-layer surface model can well represent the hard sphere surface, and to prove it, we further calculate the radial density distribution of the grafted chains on the NP with a radius of 1.5 (Fig. S1). It clearly shows that that the density value is zero for $r < 1.5$, indicating that there are no grafted chains inside the NP. Thus, it can be concluded that the grafted chains do not overlap with the NP and will not penetrate and enter the interior of the Janus NP. These results indicate that the NP we constructed is impenetrable. This method of constructing NP surface models by geodesic meshing is a method developed by our group in the early stage and has been widely used, see literature [15–18] for details. In our simulations, all beads of the NP are treated together as a rigid body. The quaternion method is applied on the beads of the same NP to constrain mutual movement of the NP-type beads in the same NP. The size of the NP is set to be 3 in DPD units, which is comparable to the thickness of the bilayer membrane. This parameter setting is mainly based on a previous study, where Alexeev et al.[7] chose NPs with a size similar to the thickness of the membrane, in order to investigate the behavior of NPs when stretching and shrinking a lipid membrane. The grafted sites are uniformly distributed on the surface of NPs. In order to enhance the interaction between the graft chains on the surface of NPs (or ensure that the graft chains can fully contact each other), we set the graft density of polymer chains on the surface of NPs as 1.0 chains/r_c^2, that is, 1.9 chains/nm^2. This graft density is easily attained in experimental studies. For example, many experimental studies [19–21] have shown that the graft density of poly(ethylene glycol) (PEG) on the surface of NPs is within the range of $0-2.0$ chains/nm^2. The ratio of hydrophobic to hydrophilic grafted sites on the NP is 1:1. The hydrophobic chain (A, red) or hydrophilic chain (B, gray) grafted on the NP is composed of several connected beads, and the number of the beads (denoted as n) varies from 5 to 10 in different simulations.

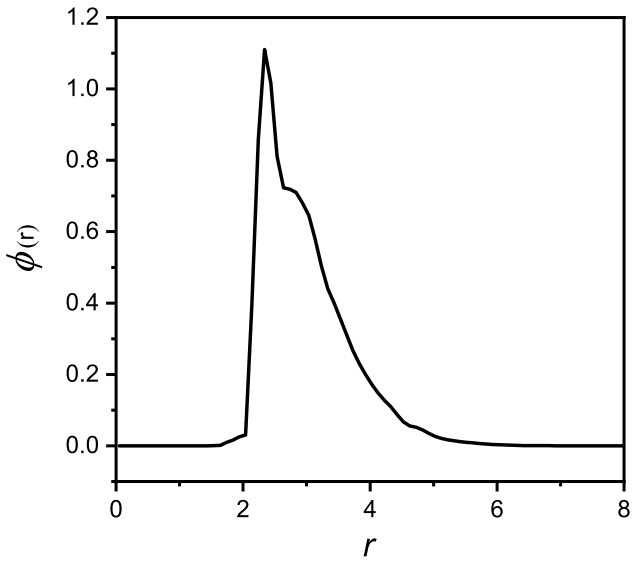

Fig. S1 Radial density distribution profile of the grafted chains on the Janus PGNP with a radius of 1.5. The hydrophobic and hydrophilic grafted chains on the PGNP have the same chain length of 5.

The interaction of the grafted polymer chains may have an effect on the rotation of the NPs. In order to investigate the effect of the grafted chains on the rotation of the NPs, we simulate the motion of the bare NP and the NP with graft chains in a $20 \times 20 \times 20$ cube box and plot their orientation correlation profiles. When taking the initial vector formed by the mass center of two Janus hemispheres as a reference vector, we calculated the dot product of the reference vector and the newly generated vector as a function of time during the motion. When the values of dot product tend to zero, it indicates that there is no orientation correlation between the reference vector and the newly generated vector. The larger the dot product value, the stronger the orientation correlation. We measure the effect of the graft chains on NP rotation by comparing the length of time it takes to reach orientation independence. As shown in Fig. S2, Janus PGNP need a longer time to reach orientation independence. Thus, the graft chains do not enhance the rotation of the NP, but rather slow it down.

We stretch and shrink the bilayer membrane by changing the lateral dimensions of the simulation box and simultaneously modify the height of the box to keep the volume of the system constant. During this process, the surface tension and stress are recorded. In our simulations, the surface tension ς and stress γ are calculated as following:

$$\varsigma = \frac{1}{2}\left\langle L_z(P_{zz} - \frac{P_{xx}+P_{yy}}{2})\right\rangle, \tag{S11}$$

$$\gamma = \frac{1}{2}(P_{xx}+P_{yy}) - \frac{1}{2}(P_{xx}+P_{yy})_{t=0}, \tag{S12}$$

where L_z is the box length along the z direction (i.e., normal to the bilayer membrane), and $P_{\lambda\lambda}$ is the diagonal component of the pressure tensor ($\lambda = x$, y, or z). The rate of stretching or shrinking is defined as

$$v = D_x/t, \tag{S13}$$

here D_x is the change in the x-direction of the simulated box and t is the total time of stretching or shrinking. We start with a tension-free membrane, and then increase the area of the box by 40% to create a pore to mimic the plasma membrane rupture. We then restore the box to its initial size at a slower rate to simulate the membrane repair process.

We would like to clarify that the membrane repair process mainly includes three steps: 1) rapid accumulation of the repair proteins at the edge of the membrane wound, helping reduce wound stress and in turn the degree of membrane damage; 2) cell proliferation or the migration of vesicle membranes in the cytoplasm to repair the damaged area; 3) the detachment of the repair proteins from the wound after membrane repair. Therefore, the repair proteins act as a regulator during the membrane repair process. In our simulation, shrinking the simulation box is used to mimic the functions of cell proliferation or the migration of vesicle membranes in the cytoplasm. As such, shrinking the simulation box can repair the pore of the damaged membrane in the absence of Janus PGNPs, but the function of the repair proteins cannot be reflected throughout the simulation. Furthermore, there are two key roles of the introduced Janus PGNPs in the repair process: 1) they are specifically adsorbed at the edge of the pore in the damaged membrane to effectively reduce the

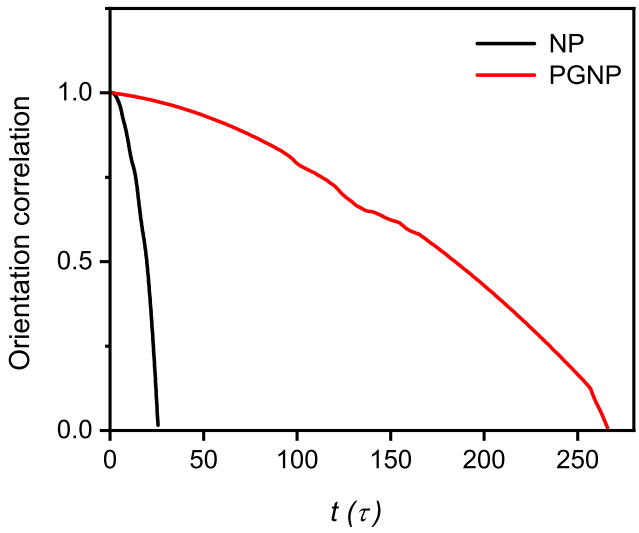

Fig. S2 The correlation of the centroid vector of the two hemispheres of a NP during particle rotation. The diameter of the NP is 3, and the length of the hydrophobic and hydrophilic grafted chains on the PGNP is 5.

membrane stress, which helps to decrease the degree of membrane damage; 2) as mentioned in the introduction, when used to mimic the function of proteins, all the reported Janus NPs were eventually embedded in membrane, which might affect the biological function of the cell membranes. This deviates from the true behavior of repair proteins. In contrast, our work shows that after the membrane is repaired, Janus PGNPs will be detached from the lipid membrane and can be reused without affecting the normal function of the membrane. Thus, our designed Janus PGNPs well mimic the functions of repair proteins.

To correlate the simulation results to physical length and time scales, we calculate the mean squared displacement (MSD) of lipid molecules in the tensionless membrane as a function of simulation time (Fig. S3), from which, we can obtain the diffusion coefficient $D = 0.011 r_c^2/\tau$. In our simulations, the area per lipid is calculated as $1.21 r_c^2$. Typical area per lipid in a tensionless DPPC membrane is about 0.61 nm^2, and an experimental measurement of the in-plane diffusion coefficient of lipids is $D = 5\mu m^2/s$ [22]. We use these values to establish the length scale and time scale in our simulations, thereby $r_c = 0.71$ nm and $\tau = 1.2$ ns.

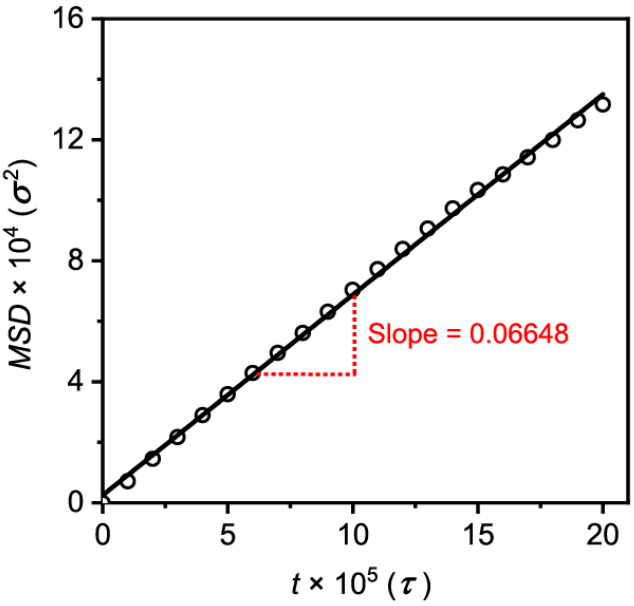

Fig. S3 Mean squared displacement (MSD) of lipid molecules in a bilayer membrane as a function of time t. The line is a best fit to the data.

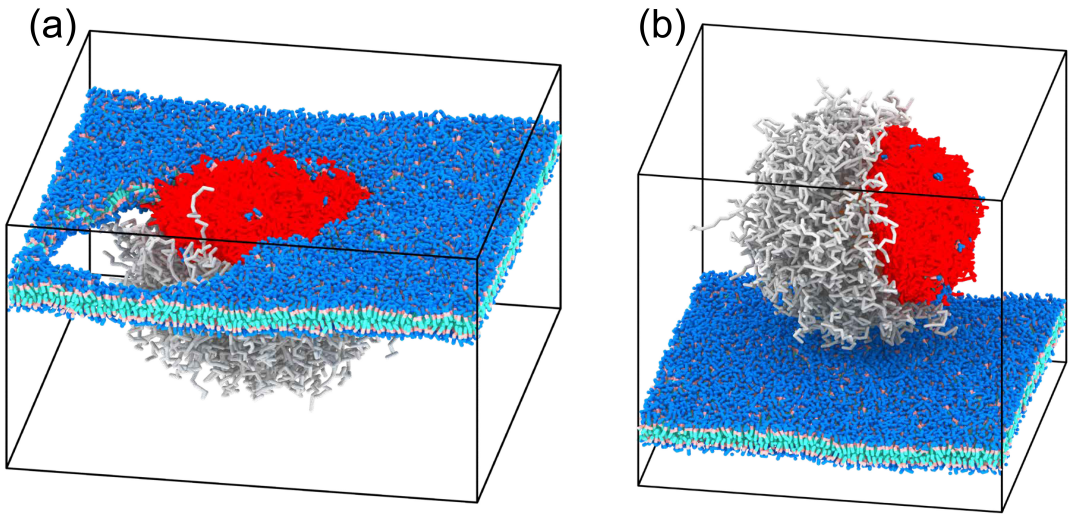

Fig. S4 (a)Side view of a stretched lipid bilayer membrane in the presence of the Janus PGNP with a radius of 7.5. The length of the hydrophobic and hydrophilic grafted chains on the PGNP is 25. The ratio of the grafted polymer length to the NP size, as well as the graft density were the same as those in Fig. 3 and Fig. 4. Solvent is not shown for clarity. (b) Side view of the lipid membrane with the Janus PGNP when the membrane returns back to its initial state. The component's color settings are the same as those in Fig. 1.

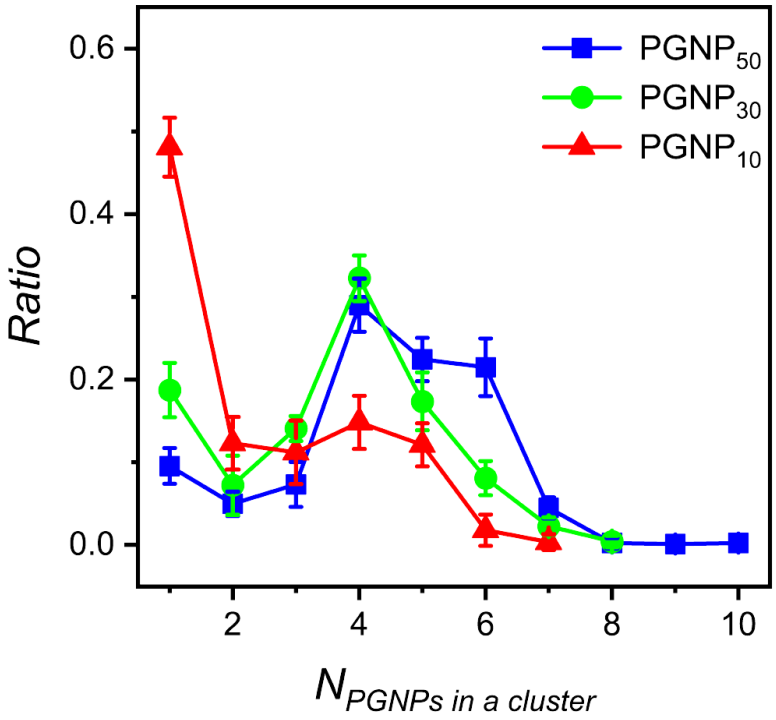

Fig. S5 The probability distribution of the number of Janus PGNPs in a cluster. $PGNP_{50}$, $PGNP_{30}$ and $PGNP_{10}$ represent that the total number of Janus PGNPs in the system is 50, 30, 10, respectively.

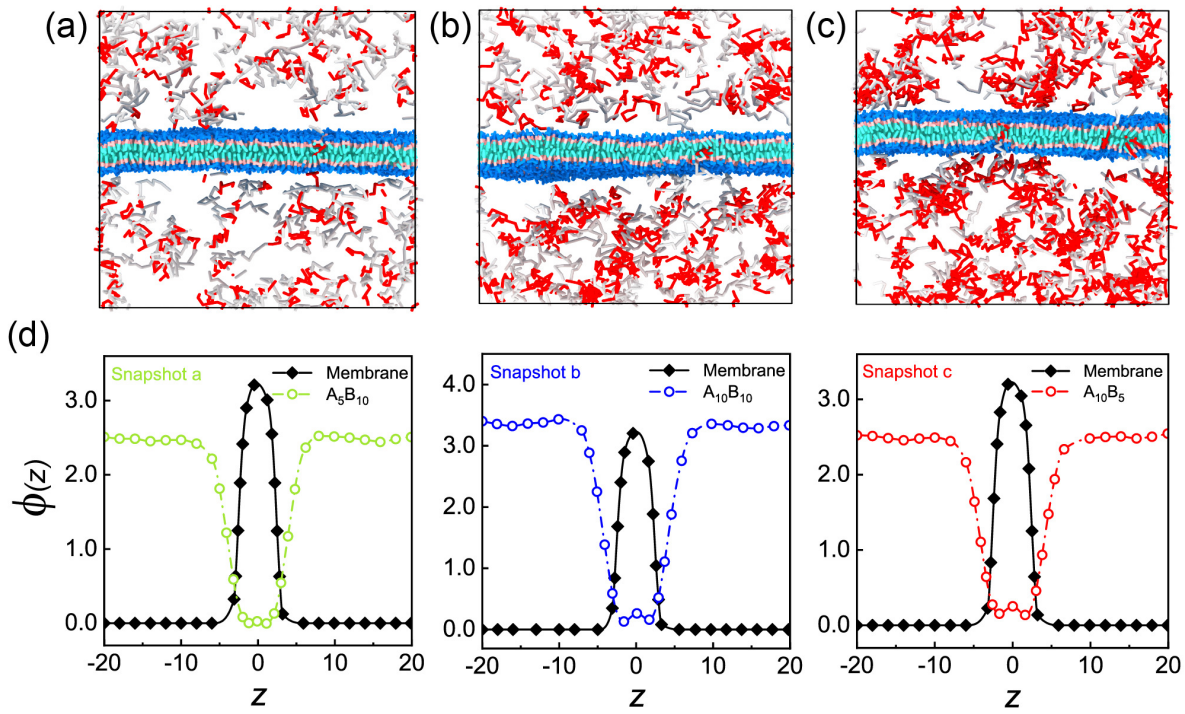

Fig. S6 (a)-(c) Snapshots for the systems with lipid membrane and block copolymers of different chain lengths and compositions, taken after the membrane stretching is released and the pore is closed: (a) A_5B_{10}, (b) $A_{10}B_{10}$ and (c) $A_{10}B_5$. A and B represent hydrophobic and hydrophilic blocks, respectively, and the subscript indicates the length of the corresponding block. These snapshots could be compared to the snapshot shown in Fig.2(d) of the paper. (d) Density profiles of the lipid membrane and block copolymers in (a)-(c). In the system, the number of block copolymer chains is equal to the total number of grafted chains in the Janus PGNPs system. The interaction parameters between the hydrophilic and hydrophobic blocks of copolymers and the membrane are the same as those of the hydrophilic and hydrophobic grafted chains of Janus PGNPs. The density profiles of block copolymers are multiplied by a factor of 30 to bring all the profiles to a comparable scale. The abscissa $z = 0$ is the position of the mass center of the membrane. In the simulation snapshots, blue beads represent lipid head, while pink and cyan beads represent lipid tail. The gray and red lines represent the hydrophilic and hydrophobic blocks of the block copolymer, respectively. The solvent beads are omitted here for clarity.

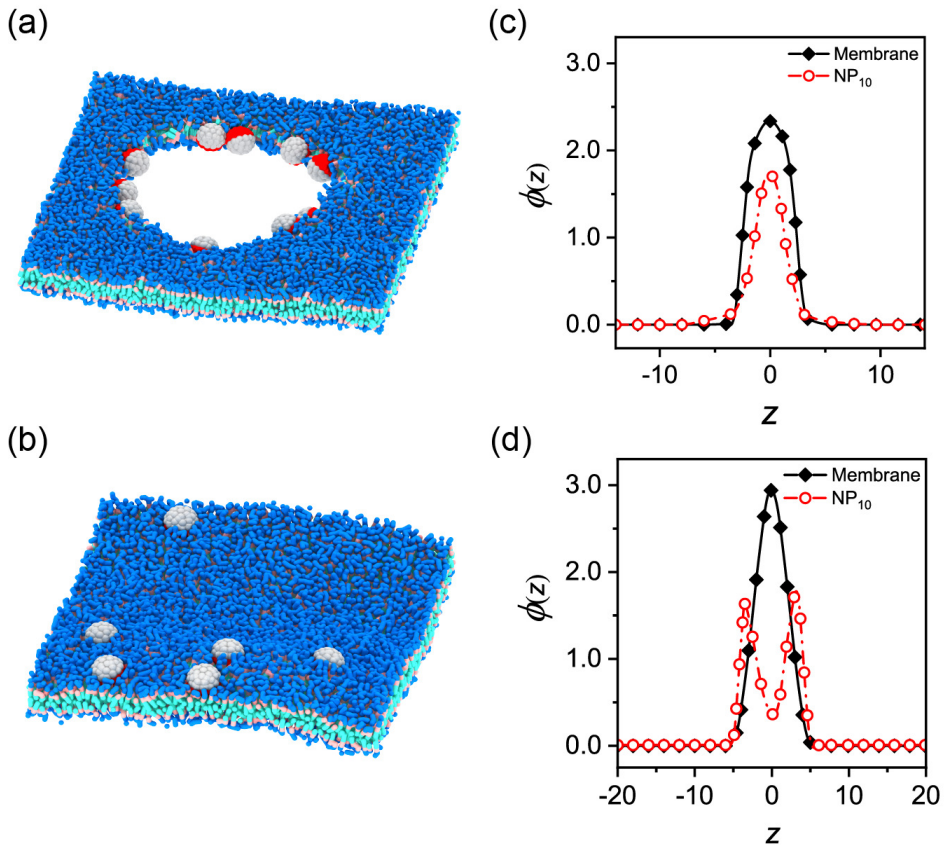

Fig. S7 (a) Snapshot of a stretched lipid bilayer membrane in the presence of 10 Janus NPs. (b) Snapshot of the lipid membrane with Janus NPs when the membrane stretching is released and the pore is closed. (c) and (d) show the density profiles of the lipid membrane and Janus NPs in (a) and (b), respectively. In the system, the interaction parameters between the hydrophilic and hydrophobic parts of Janus particles and the membrane are the same as those of the hydrophilic and hydrophobic grafted chains of Janus PGNPs. The density profiles of Janus NPs are multiplied by a factor of 1500 to bring all the profiles to a comparable scale. The abscissa $z = 0$ is the position of the mass center of the membrane. In the simulation snapshots, blue beads represent lipid head, while pink and cyan beads represent lipid tail. The gray color and red color represent the hydrophilic and hydrophobic parts of the Janus NPs, respectively. The solvent beads are omitted here for clarity.

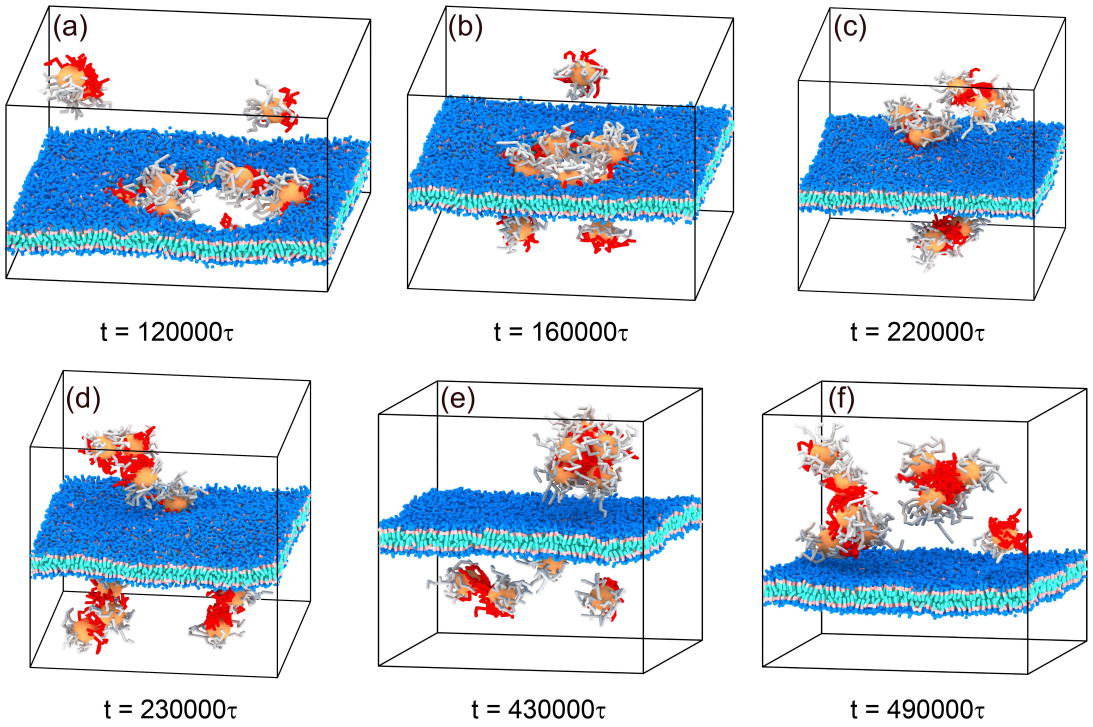

Fig. S8 Snapshots for the detachment process of Janus PGNPs from the lipid membrane via laterally shrinking the pore at a rate of 2.3 $\mu m^2/s$. The corresponding simulation time t is indicated below each snapshot. In this figure, t = 120000τ is the time when the membrane begins to shrinking, and the shrinking process lasts for 100000τ. The lengths of the hydrophobic chain and hydrophilic chain grafted on the NPs are both equal to 5. In the simulation snapshots, solvent is not shown for clarity and the component's color settings are the same as those in Fig. 1.

References

1 R. D. Groot and P. B. Warren, *J. Chem. Phys.*, 1997, **107**, 4423–4435.
2 K. Yang and Y. Q. Ma, *Nat. Nanotechnol.*, 2010, **5**, 579–583.
3 R. K. Raya, M. Štěpánek, Z. Limpouchová, K. Procházka, M. Svoboda, M. Lísal, E. Pavlova, A. Skandalis and S. Pispas, *Macromolecules*, 2020, **53**, 6780–6795.
4 P. J. Hoogerbrugge and J. M. V. A. Koelman, *Europhys. Lett.*, 1992, **19**, 155–160.
5 P. Español and P. Warren, *Europhys. Lett.*, 1995, **30**, 191–196.
6 R. D. Groot and T. J. Madden, *J. Chem. Phys.*, 1998, **108**, 8713–8724.
7 A. Alexeev, W. E. Uspal and A. C. Balazs, *Acs Nano*, 2008, **2**, 1117–1122.
8 Q. S. Xia, H. M. Ding and Y. Q. Ma, *Nanoscale*, 2017, **9**, 8982–8989.
9 Q. S. Xia, T. Zhu, Z. Y. Jiang, H. M. Ding and Y. Q. Ma, *Nanoscale*, 2020, **12**, 7804–7813.
10 S. D. Ni, Y. W. Yin, X. L. Li, H. M. Ding and Y. Q. Ma, *Langmuir*, 2019, **35**, year.
11 K. Yang and Y. Q. Ma, *Nat. Nanotechnol*, 2010, **5**, 579–583.
12 D. Xu, L. Zhao, K. Zhang and Z. Y. Lu, *Sci. China Chem.*, 2019, **62**, 1666–1674.
13 H. M. Gao, R. Shi, Y. L. Zhu, H. J. Qian and Z. Y. Lu, *Chem. Res. Chinese U.*, 2022, **38**, 653–670.
14 R. D. Groot and T. J. Madden, *J. Chem. Phys.*, 1998, **108**, 8713–8724.
15 H. Liu, Y. L. Zhu, J. Zhang, Z. Y. Lu and Z. Y. Sun, *ACS Macro Lett.*, 2012, **1**, 1249–1253.
16 B. Y. Li, Y. C. Li and Z. Y. Lu, *J. Phys. Chem. Lett.*, 2020, **11**, 4542–4547.
17 H. M. Gao, H. Liu, H. J. Qian, G. S. Jiao and Z. Y. Lu, *Phys. Chem. Chem. Phys.*, 2018, **20**, 1381–1394.
18 J. Lu, Y. Xue, R. Shi, J. Kang, C. Y. Zhao, N. N. Zhang, C. Y. Wang and K. Lu, Z. Y.and Liu, *Chem. Sci.*, 2019, **10**, 2067–2074.
19 E. Oh, J. B. Delehanty, K. E. Sapsford, K. Susumu, R. Goswami, J. B. Blanco-Canosa, P. E. Dawson, J. Granek, M. Shoff, Q. Zhang *et al.*, *ACS Nano*, 2011, **5**, 6434–6448.
20 A. Malugin and H. Ghandehari, *J. Appl. Toxicol.*, 2010, **30**, 212–217.
21 C. D. Walkey, J. B. Olsen, H. B. Guo, A. Emili and W. C. Chan, *J. Am. Chem. Soc.*, 2012, **134**, 2139–2147.
22 J. C. Shillcock and R. Lipowsky, *Nat. Mater.*, 2005, **4**, 225–228.